ISSN 2720-3581

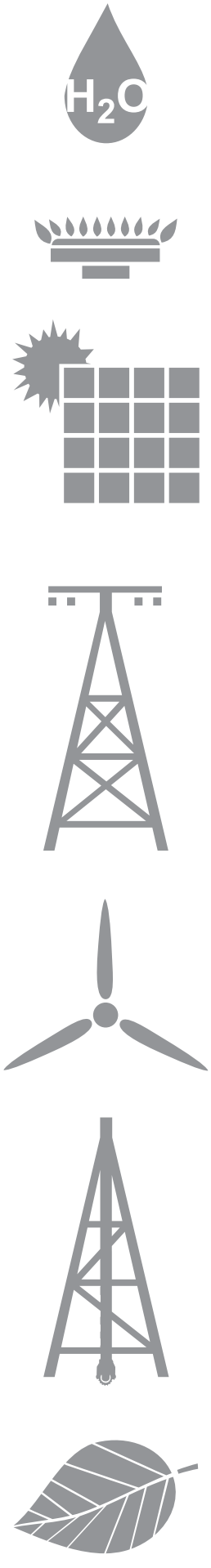

JOURNAL OF GEOTECHNOLOGY AND ENERGY

FORMERLY AGH DRILLING, OIL, GAS

2021, vol. 38, no. 3

WYDAWNICTWA AGH

KRAKOW 2021

The "Journal of Geotechnology and Energy" (formerly "AGH Drilling, Oil, Gas") is a quarterly published by the Faculty of Drilling, Oil and Gas at the AGH University of Science and Technology, Krakow, Poland. Journal is an interdisciplinary, international, peer-reviewed, and open access. The articles published in JGE have been given a favorable opinion by the reviewers designated by the editorial board.

Editorial Team

Publisher

AGH University of Science and Technology Press

Linguistic corrector: *Aeddan Shaw*
Technical editor: *Kamila Zimnicka*
Desktop publishing: *Munda*
Cover design: *Paweł Sepielak*

ISSN: 2720-3581
DOI: https://doi.org/10.7494/jge

Journal website: https://journals.agh.edu.pl/jge

Wydawnictwa AGH (AGH University of Science and Technology Press)
al. A. Mickiewicza 30, 30-059 Kraków
tel. 12 617 32 28, 12 636 40 38
e-mail: redakcja@wydawnictwoagh.pl
http://www.wydawnictwoagh.pl
http://www.wydawnictwo.agh.edu.pl

CONTENTS

Journal of Geotechnology and Energy | vol. 38 | no. 3 | 2021 | pp. 5–12

https://doi.org/10.7494/jge.2021.38.3.5

Krzysztof Polański

ORCID: 0000-0002-6604-9080
AGH University of Science and Technology

DETERMINATION OF MECHANICAL PARAMETERS OF SALTS IN THE CYCLIC LOAD PROCESSES CORRESPONDING TO THE OPERATION OF A STORAGE CAVERN FOR HYDROGEN

Date of submission:
5.10.2021

Date of acceptance:
21.10.2021

Date of publication:
31.10.2021

https://journals.agh.edu.pl/jge

Abstract: The paper describes the results of laboratory tests of the strength of salt samples made as part of the HESTOR project in order to determine the mechanical parameters of salt. The tests were carried out using an Autolab 2000 apparatus which allows to simulate any load cycles. The tests were made by simulating the operation of the hydrogen storage cavern. In order to observe the differences in salt behavior depending on the sample medium being stored during the test, gases were supplied: nitrogen, as an analogue of natural gas, and helium as a hydrogen analogue.

Keywords: salt, hydrogen, storage cavern, energy storage in the hydrogen

1. Introduction

Strength tests to determine the mechanical parameters of salt were made using an Autolab 2000. The tests were carried out for both the "pure" salt sample and the samples to which nitrogen was supplied, as an analogue of natural gas and helium as a hydrogen analogue [1].

Autolab 2000 is a specialist apparatus for testing the strength and petrophysical properties of rock samples, enabling the implementation of any load scenario in a triaxial stress system. The apparatus allows the examination of samples with a maximum core diameter of 102 mm (4 inches) and a length of up to 177.8 mm (7 inches). The maximum axial load on the tested core is up to 1890 kN, with the maximum sealing pressure up to 140 MPa. The maximum pore pressure in the core under test is also 140 MPa [2].

Measurements of mechanical properties of salt samples cut from selected locations consisted of placing a sample prepared in the form of a cylinder with a diameter of 1.5 inch and a height of 3–3.5 inch, so that the slenderness 2 (the height of the sample to its diameter) was preserved, in a special rubber flange, which from the bottom and top is closed with steel pivots. Special rings are mounted on them to place the LVDT sensors around the sample, and then place it in the apparatus. The prepared salt sample is placed on the apparatus table (presented in Fig. 1) to which LVDT sensors are connected, which makes it possible to read the sensors in real-time using specialized software [2].

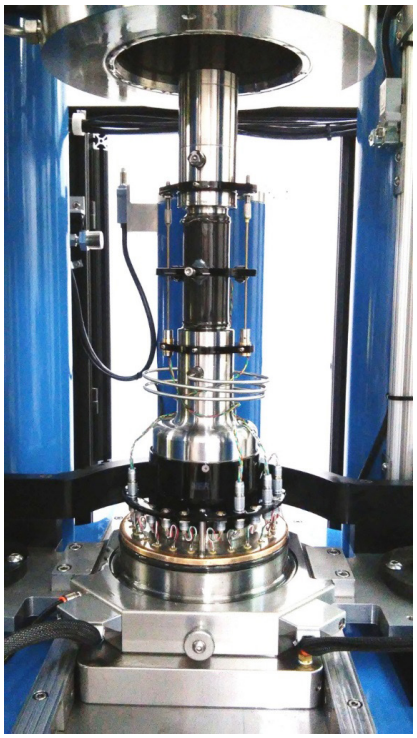

Fig. 1. The prepared salt sample during placement in the Autolab 2000 measuring cylinder

The sample placed on the table is closed into the pressure chamber of the apparatus. The chamber is filled with oil which creates peripheral pressure (seal pressure) around the sample. Then, by controlling the movable piston, pressure is applied to the salt sample previously described by distances, whereby the axial stresses in the test sample are induced. On the basis of readings from linear and peripheral strain sensors, the computer software processes the obtained results. Thanks to this it is possible to determine mechanical parameters during a given measurement cycle [2].

2. Laboratory tests of mechanical parameters of samples of salt cores as an elastic-plastic-viscous medium in cyclic load processes

To perform laboratory tests of mechanical properties, samples were selected from three different locations of the Polkowice-Sieroszowice Mine, representing various crystallographic salt structures [3–6]. Samples were made in the form of a cylinder with a diameter of 38.1 mm (1.5 inch) and a height of approx. 86 mm (3.4 inch), which were adjusted to the requirements of the Autolab 2000 apparatus [2].

The following sample description scheme was adopted: PS7, US2, SG2 indicates the location from which the given sample originated. Roman number I, II, III indicate the number of the sample that has been tested. The Arabic number 1, 2, 3 indicates the next test number for the given sample. Investigations of mechanical properties of salts from selected locations were conducted in short-term load cycles using the same scenario for selected samples. In the case of samples where no gas was supplied, a confining pressure was set to 10 MPa.

For samples where gas (nitrogen or helium) was supplied at pressure 5 MPa, the confining pressure was increased to 15 MPa to maintain the same test conditions as for the "clean" samples. For all samples, the vertical pressure was set at the beginning of the test so that the piston loading the sample adhered to it but did not load it – without any initial deformation.

The test scenario was as follows: after setting the confining pressure (and the saturation pressure), the salt sample was left until the deformations observed in the graph (live data) showing that the sensors remained unchanged. Depending on the sample, it took 0.5–2.5 h. In the next step, the axial load of the sample was set by

changing the pressure exerted by the piston loading the sample (the pressure exerted by the piston). The amplitude of this load was 4 MPa. After reaching 4 MPa, the load was removed. For the tests, a load speed of 0.006 MPa/s was adopted, i.e. the loading time was 666.7 s and the same unloading time. In order to compare the impact of the speed of a given load on the obtained results, during the tests it was decided that for one load of the same sample, a 10× speed higher, i.e. 0.06 MPa/s, would be used. The loading time of the sample in this case was therefore 66.7 s and the same unloading time. Each of the tested samples was loaded 3 times, with a 48–72 hour period between successive loads. At that time, the sample was removed from the apparatus – unloaded.

It should be emphasized that the adopted research scenarios assumed non-destructive testing, as the samples used were to be comparably tested to determine permeability. Therefore, the tests were performed in the lower range of loads used for salt, which translates into Young's modules being obtained which belong to this load range. At higher loads and relieves, the values obtained can be greater, even five times as much.

The tests were performed using LVDT (Linear Variable Displacement Transducer Test) sensors. These sensors operate on the principle of an induction coil producing 0–10 V voltage. Through the software, the signal from the sensors is converted into a displacement value. Each time the prepared sample was placed on the Autolab 2000 table, the LVDT sensors were calibrated by placing the sensor core as close as possible to the center of the coil. The calibration was made by setting a voltage close to 1.5 V for axial sensors and a value close to 5 V for a radial sensor, so that the range of sensor readings was as large and as accurate as possible. However, the high sensitivity of the sensors means that even after the calibration is carried out directly on the sample, there is the phenomenon of "initial deformation" of the sample that can also be caused by the reaction of the sensors to apply the initial axial pressure to the sample (touching the sample by the loading piston).

During the test, the readings of deformation values of samples from 2 linear strain sensors (LVDT1, LVDT2) and a radial strain sensor (LVDT3) were carried out. The examples of data from LVDT sensors obtained during testing are shown in the diagrams presented in Figures 3, 5 and 7. With the use of LVDT sensors, the computer software allows the reading of axial deformations (change of sample height) and radial (change of sample diameter) as the ratio of the sample height/diameter (before the start of the test) to the current value of this parameter.

$$\varepsilon = \frac{\Delta l}{l} \tag{1}$$

The accuracy of LVDT sensors allowed us to obtain results with an accuracy of 10^{-16}, hence the unit in which the presented results in the graphs is "1mε" (as described in the Autolab 2000 charts), i.e. 1‰. On the basis of readings from sensors inside the apparatus allowing control over the pressure loading the sample, the software automatically determines the values of the Young's modulus and Poisson's coefficient for the tested sample. In combination with the high sensitivity of LVDT sensors, the Autolab 2000 apparatus allows the values of these coefficients to be obtained with an accuracy of 10^{-9}, however for the purpose of determining these parameters for salt, such high accuracy is not required, hence the accuracy of these 10^{-3} values in the results presented in Tables 1–3 [2].

3. Test results

Sample PS7

Sample PS7 is presented in Figure 2. This is a very clean sample with large salt crystals, a white-colored crystal. The halite crystals have sizes up to 3 cm. Their outlines are xenomorphic, uneven and show no elongation. Occasionally, pollutants appear in the form of small anhydrite streaks distributed along the boundaries of the halite crystals [5].

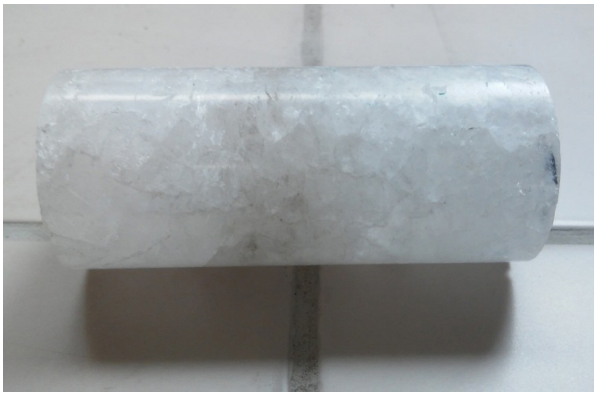

Fig. 2. Sample PS7 – halite crystals have sizes up to 3 cm. Their outlines are xenomorphic and showing no elongation

The example of deformation diagram obtained during the tests of samples PS7 are presented on Figure 3. The diagram include direct readings from sensors LVDT1, LVDT2 (axial deformations – decrease of the sample height), LVDT3 (radial deformations – reduction of the sample diameter). When comparing individual diagrams, it can be noticed that axial deformations

during the tests for samples from this location did not exceed 0.3‰. After unloading the sample, its total strain did not exceed 0.15‰. However, radial deformations only occurred when the maximum load of the sample was reached. After relieving the samples, they returned to their original level.

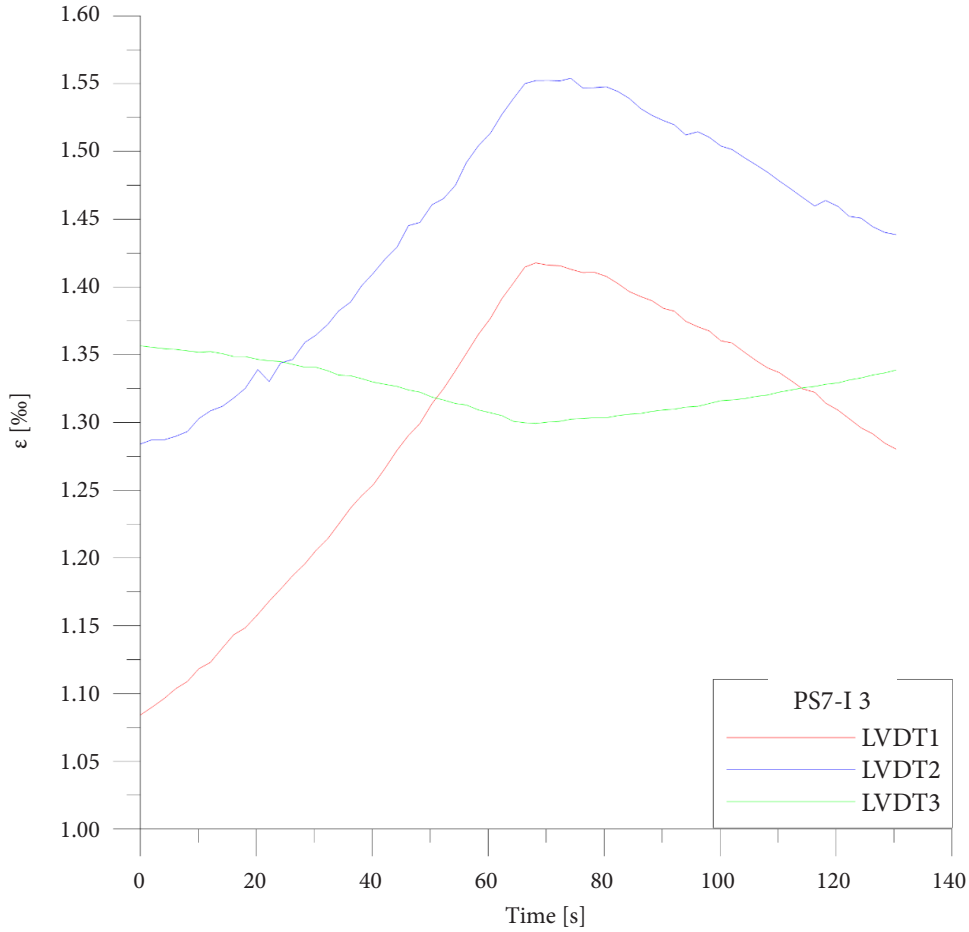

Fig. 3. The reading diagram from sensors LVDT 1, 2, 3 obtained during the test for sample PS7-I 3

Table 1. Results obtained during testing the PS7 sample

Sample	Sample diameter [mm]	Sample height [mm]	ν	E [GPa]	Tempera-ture [°C]	Pore pressure [MPa]	Confining pressure [MPa]	Gas in the pores	Loading speed [MPa/s]
Ps7-I 1	38.15	86.85	**0.205**	**13.790**	16.809	0.00	10.175	none	0.006
Ps7-I 2	38.15	86.85	**0.133**	**8.659**	16.311	0.00	10.153	none	0.006
Ps7-I 3	38.15	86.85	**0.181**	**9.605**	16.113	0.00	10.153	none	0.06
Ps7-II 1	38.10	86.80	**0.225**	**26.989**	17.145	5.00	15.186	N_2	0.06
Ps7-II 2	38.10	86.80	**0.229**	**26.824**	16.347	5.00	15.181	N_2	0.06
Ps7-II 3	38.10	86.80	**0.207**	**20.866**	16.604	5.00	15.173	N_2	0.006
Ps7-III 1	38.05	86.65	**0.230**	**21.162**	16.563	5.00	15.185	He	0.06
Ps7-III 2	38.05	86.65	**0.235**	**15.793**	16.873	5.00	15.191	He	0.006
Ps7-III 3	38.05	86.65	**0.248**	**21.197**	16.2996	5.00	15.174	He	0.06

In samples from the PS7 location (Tab. 1), Poisson's values obtained during tests of "clean" and gas-saturated samples fluctuated in the range of 0.13–0.24, while the Young's modulus for samples without saturation varies between 8.65–13.78 GPa. For samples "with helium": 15.7–21.19 GPa, and the highest value was obtained for samples which were saturated with nitrogen: 20.86–26.98 GPa.

On the basis of the obtained results, it can be concluded that the gas saturation has no effect on the change of the Poisson coefficient, while the salt subjected to gas saturation shows an increase in the Young's modulus. The spread of the obtained results, both for nitrogen and helium, does not allow for unambiguous confirmation of whether the type of gas used affects the differences in the Young's modulus obtained.

Sample US2

This sample is presented in Figure 4. It is a light gray, medium and coarse crystalline salt with halite crystals up to 1 cm. A rock with a random texture, in places the halite crystals have a slight elongation. After a few hits the sample becomes crumbly, "sugary" [7].

Fig. 4. Sample from the US2 location – in the picture visible light gray, medium-crystalline salt construction

The example graph of deformations of samples from the US2 location during the tests are presented in Figure 5. The deformation scale for US2 samples does not exceed 0.3‰ relative to the state at the beginning of the load cycle.

It should be noted that the LDVT1, LDVT2 diagrams for US2 and 1, 2, 3 trials show only a very low amplitude, which is due to the large y-axis range. The large "initial deformation" of the US2-I sample is probably caused by inaccurate calibration of the sensors before the start of the test, hence the high "initial strain" value for this sample [8].

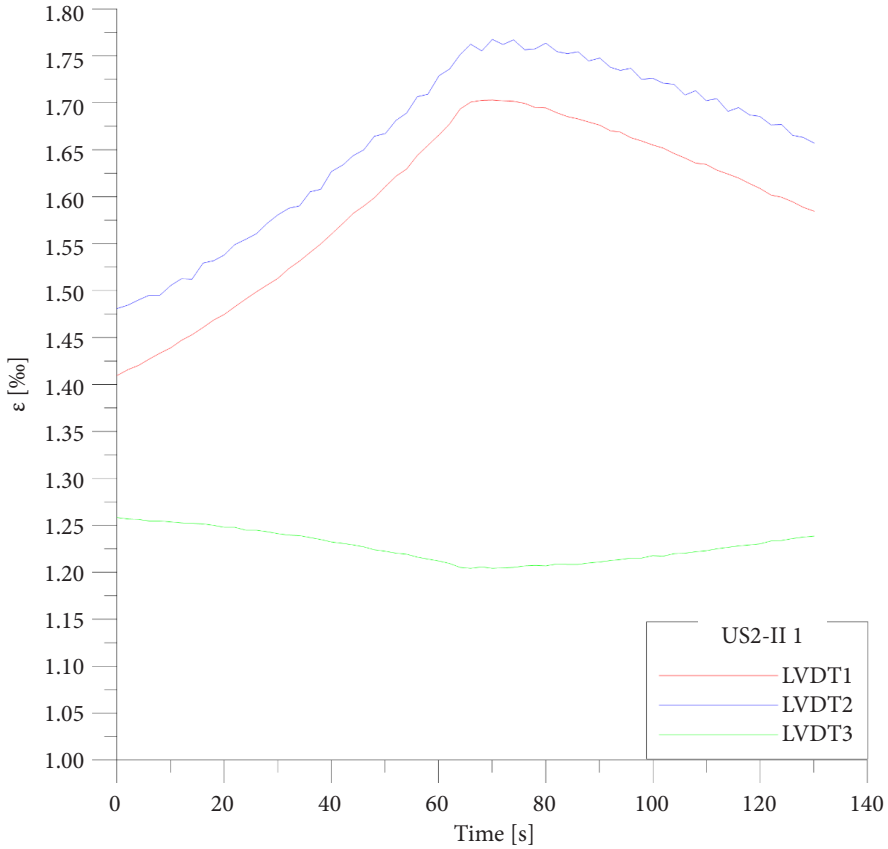

Fig. 5. The reading diagram from sensors LVDT 1, 2, 3 obtained during the test for sample US2-II 1

Table 2. Results obtained during testing the US2 sample

Sample	Sample diameter [mm]	Sample height [mm]	ν	E [GPa]	Temperature [°C]	Pore pressure [MPa]	Confining pressure [MPa]	Gas in the pores	Loading speed [MPa/s]
US2-I 1	38.05	86.00	**0.303**	**6.361**	17.189	5.00	12.226	N_2	0.06
US2-I 2	38.05	86.00	**0.304**	**4.137**	17.550	5.00	15.254	N_2	0.006
US2-I 3	38.05	86.00	**0.323**	**5.792**	17.431	5.00	15.272	N_2	0.006
US2-II 1	38.50	88.25	**0.181**	**9.624**	16.921	5.00	15.254	He	0.06
US2-II 2	38.50	88.25	**0.250**	**12.661**	17.000	5.00	15.222	He	0.06
US2-II 3	38.50	88.25	**0.208**	**7.205**	16.436	5.00	15.230	He	0.006
US2-III 1	38.15	85.75	**0.268**	**11.776**	16.851	0.00	10.163	none	0.06
US2-III 2	38.15	85.75	**0.298**	**8.108**	16.482	0.00	10.167	none	0.006
US2-III 3	38.15	85.75	**0.310**	**14.494**	16.661	0.00	10.177	none	0.006

For the "clean" samples from US2 location (Tab. 2), Poisson's ratios of 0.26–0.31 were obtained, for samples saturated with nitrogen: 0.30–0.32, while for helium-saturated samples, the values of this coefficient varied within 0.18–0.25.

The Young's modulus values were respectively: 8.1–14.5 GPa for "pure" samples, 4.13–6.36 GPa for samples saturated with nitrogen, 7.2–12.66 GPa for samples saturated with helium. On the basis of the obtained results, in the case of Poisson's coefficient one can notice a slight decrease in its value with samples with helium. However, on the basis of the value of this coefficient obtained for the "pure" and saturated with nitrogen, the effect of gas saturation on the change of the Poisson coefficient cannot be confirmed.

In the case of Young's modulus, the lowest values of this parameter were obtained for samples saturated with nitrogen, which may indicate a weakening of the geomechanical properties of salts under the influence of gas. However, already the comparison of the values obtained for "pure" and helium samples, the differences in the values of this parameter are not so clear and do not allow unambiguous confirmation of this conclusion.

Sample SG2

A sample of white or light gray medium crystals with a random texture (Fig. 6). The sample is similar to sample US2, and after a few hits it becomes scattered. The halite crystals have sizes of about 3 to 7 mm [7].

A sample deformation diagram obtained during the tests of samples from the SG2 location is presented in Figure 7. When comparing individual diagrams, it can be noticed that the scale of axial deformations during the tests, for samples from this location did not exceed 0.3‰, while radial deformations for SG2 samples were practically non-existent.

For the "clean" samples from SG2 location (Tab. 3), Poisson's values of 0.05–0.10 were obtained, for samples saturated with nitrogen: 0.13–0.21, while for samples saturated with helium, values of this coefficient were obtained: 0.13–0.22. In the case of Young's modulus, the values were respectively: 13.05–14.06 GPa for "pure" samples, 19.98–25.12 GPa for nitrogen saturated samples and 22.23–30.62 GPa for helium saturated samples.

Fig. 6. Salt sample SG2. The picture shows a disorderly, medium-crystalline salt structure

In the case of samples from this location, a large difference in the obtained parameter values is noticeable compared to the tested salt samples from other locations. This may be due to the significant differences

in the mechanical properties of the salt from this location, which can be influenced by inclusions inside all of the salt samples from this location. In the case of samples saturated with nitrogen and helium, there is also a clear increase in the value of the tested parameters, however, based on the conducted tests it is impossible to clearly indicate whether the type of gas used affects the values obtained.

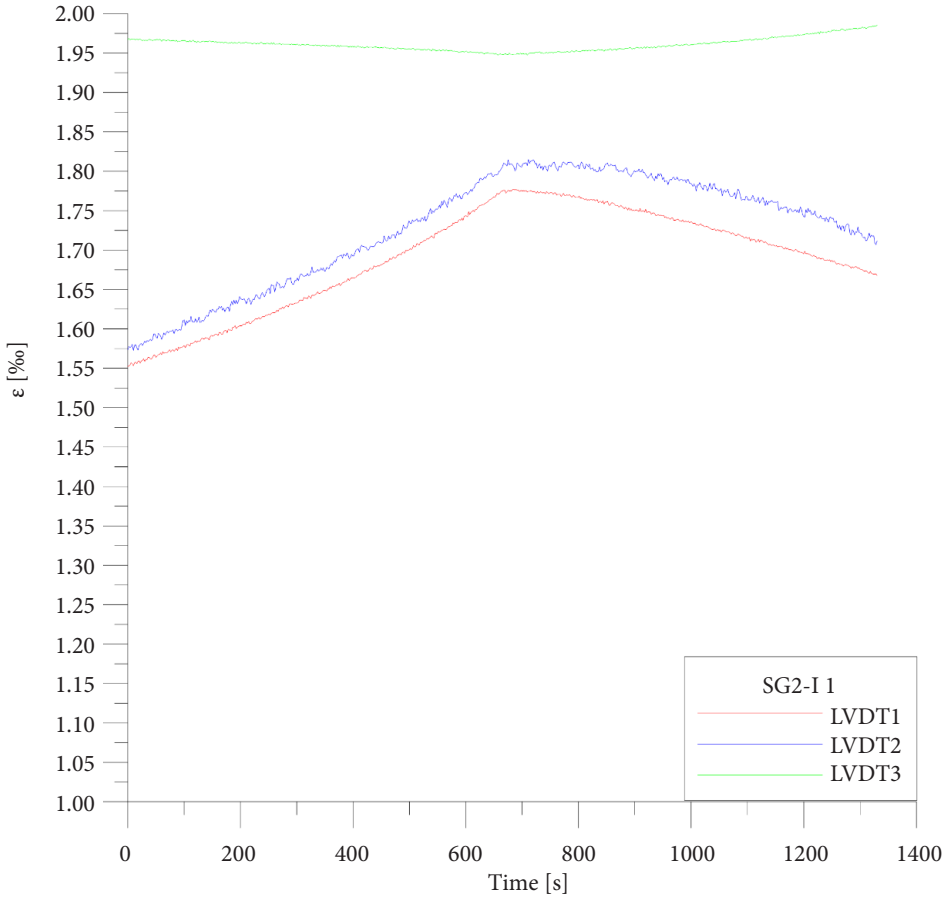

Fig. 7. The reading diagram from sensors LVDT 1, 2, 3 obtained during the test for sample SG2-I 1

Table 3. Results obtained during testing the SG2 sample

Sample	Sample diameter [mm]	Sample height [mm]	ν	E [GPa]	Temperature [°C]	Pore pressure [MPa]	Confining pressure [MPa]	Gas in the pores	Loading speed [MPa/s]
SG2-I 1	38.05	86.02	**0.056**	**13.377**	17.278	0.00	10.205	none	0.006
SG2-I 2	38.05	86.02	**0.105**	**14.060**	17.142	0.00	10.200	none	0.06
SG2-I 3	38.05	86.02	**0.096**	**13.058**	16.101	0.00	10.145	none	0.06
SG2-II 1	38.15	85.8	**0.132**	**23.176**	15.667	5.00	15.188	N_2	0.006
SG2-II 2	38.15	85.8	**0.163**	**19.984**	17.689	5.00	15.251	N_2	0.006
SG2-II 3	38.15	85.8	**0.215**	**25.120**	13.584	5.00	15.101	N_2	0.06
SG2-III 1	38.17	86.91	**0.156**	**30.615**	17.149	5.00	15.204	He	0.006
SG2-III 2	38.17	86.91	**0.134**	**22.231**	16.175	5.00	15.195	He	0.006
SG2-III 3	38.17	86.91	**0.218**	**26.785**	12.933	5.00	15.121	He	0.06

4. Conclusions

The results of mechanical properties tests for samples from the US2 location confirm the average values of the Young's Module obtained so far in uniaxial mechanical tests ($E \approx 8$ GPa). However, for samples from the location of SG2, PS7, higher values of the Young's modulus were obtained, which may be due to the overly large number of crystals in relation to the total size of the tested sample or/also a larger number of anhydrite inclusions inside the salt samples.

During the tests, the long relaxation time of the salt was indirectly confirmed – for the tested samples at the repetition of the load cycle even after 2–3 days higher values of the Young's modulus were obtained. It may also be due to stress reinforcement of the sample. On the other hand, the Poisson ratio was similar for each specific sample.

During the determination of the Poisson ratio, similar values were obtained for the majority of samples ranging from 0.1 to 0.3. This may indicate that the construction of salt crystallographic salt does not directly affect the value of this coefficient [9].

During the tests carried out with the use of two sample loading speeds (0.006 MPa/s and 0.06 MPa/s), no unambiguous effect of the speed of the given load on the obtained values of mechanical parameters of the tested samples was observed.

The results of laboratory tests of mechanical properties with nitrogen and helium saturation did not show significant differences in the mechanical parameters tested. It confirms that it is possible to store hydrogen in salt caverns and the storage will not be significantly different from the case of natural gas storage [10].

Funding: This research was funded by National Centre for Research and Development (Grant No. GEKON1/O2/214140/23/2015).

Acknowledgments: The author would like gratefully acknowledge the financial support from the National Centre for Research and Development (Grant No. GEKON1/O2/214140/23/2015).

References

[1] Schlichtenmayer M., Bannach A.: *Renewable Energy Storage in Salt Caverns – Behavior Comparison of Methane, Hydrogen and Air in Rock Salt*. SMRI Research Project Report RR2015-1, 2015. Freiberg, Germany.

[2] Polański K., Serbin K., Smulski R., Wiśniowski R., Stryczek S., Urbańczyk K., Burliga S., Lankof L., Kuźniar-Klimkowska A., Węgrzynek A., Piotrowski M.: *Magazynowanie energii w postaci wodoru w kawernach solnych, Zadanie 3: Badania laboratoryjne i in-situ dla określenia warunków szczelności kawerny magazynowej. Sprawozdanie z prac wykonanych w okresie II 2015–IX 2017 przez zespół Akademii Górniczo-Hutniczej im. Stanisława Staszica w Krakowie*. Kraków 2017, pp. 83–126.

[3] Burliga S.: *Internal structure of subhorizontal bedded rock salt formation in the area of Sieroszowice – meso- and micro-structural investigations*. Gospodarka Surowcami Mineralnymi, vol. 23, 2007, pp. 51–64.

[4] Kłeczek Z., Zeljaś D.: *Naukowe podstawy i praktyczne zasady budowy w Polsce podziemnego składowiska odpadów niebezpiecznych (Scientific basis for and practical principles of construction Poland underground repository of hazardous waste)*, [in:] R. Zając (red.), *Innowacyjne techniki i technologie mechanizacyjne. Monografia*. Instytut Techniki Górniczej KOMAG, Gliwice 2012, vol. 12, pp. 217–219.

[5] Ślizowski J., Urbańczyk K., Lankof L., Serbin K.: *Analiza zmienności polskich pokładów soli kamiennej w aspekcie magazynowania gazu*. Wiertnictwo, Nafta, Gaz, vol. 28, no. 1–2, 2011, pp. 431–443.

[6] Ślizowski J., Wojtuszewska K., Wiśniewska M.: *Pojemność komór magazynowych gazu w pokładowych złożach soli na monoklinie przedsudeckiej*. Zeszyty Naukowe IGSMiE PAN, 2009, pp. 5–11.

[7] Stasik I.: *W sprawie nomenklatury, terminologii i nazewnictwa skał solnych*. Przegląd Geologiczny, vol. 36, no. 5, 1988, pp. 294–297.

[8] Zeljaś D.: *Własności reologiczne soli kamiennej złoża monokliny przedsudeckiej – Rheological properties salt seam of Sudetic Monocline*, [in:] A. Klich, A. Kozieł (red.), *Innowacyjne i przyjazne dla środowiska techniki i technologie przeróbki surowców mineralnych: bezpieczeństwo – jakość – efektywność: praca zbiorowa: monografia*. Instytut Techniki Górniczej KOMAG, Gliwice 2011, pp. 257–267.

[9] Zeljaś D.: *How to localize an Underground Gas Storage (UGS) in a salt structure of the Fore-Sudetic Monocline in light of its geomechanical properties*. AGH Drilling, Oil, Gas, vol. 33, no. 4, 2016, pp. 699–711.

[10] Ślizowski J., Smulski R., Nagy S., Burliga S., Polański K.: *Tightness of hydrogen storage caverns in salt deposits*. AGH Drilling, Oil, Gas, vol. 34, no. 2, 2017, pp. 397–409.

Journal of Geotechnology and Energy | vol. 38 | no. 3 | 2021 | pp. 13–18

https://doi.org/10.7494/jge.2021.38.3.13

Krzysztof Machocki
ORCID: 0000-0002-1920-1916
Aramco Overseas Company

Ossama Sehsah
ORCID: 0000-0001-8953-7768
Saudi Aramco

Zahrah Marhoon
ORCID: 0000-0002-4369-7253
Saudi Aramco

Tom Dixon
ORCID: 0000-0002-1596-0704
Electro-Flow Controls

Shaarawi Amjad
ORCID: 0000-0002-2350-3300
Saudi Aramco

Jamal Ud-Din Mohammad
ORCID: 0000-0001-8208-2123
Weatherford

A NEW NON-INTRUSIVE CONDITION MONITORING SYSTEM DESIGNED TO IMPROVE RELIABILITY OF RCDs

Date of submission:
4.10.2021

Date of acceptance:
19.10.2021

Date of publication:
31.10.2021

https://journals.agh.edu.pl/jge

Abstract: Managed Pressure Drilling (MPD) is a technology that allows for precise well-bore pressure control, especially in formations with uncertain geomechanics. The Rotating Control Device (RCD) is a crucial part of the MPD equipment but is prone to failure. Therefore, a new condition monitoring system was developed to improve the reliability of RCDs and eliminate their catastrophic failures during MPD jobs. Non-intrusive sensors were selected during the design of this condition monitoring system. Sensors measure: vibrations, acoustic emissions, rotation, pipe movement, temperatures, and contamination level in the coolant fluid. The system can display the measurements in real-time to the operator, giving early warnings to prevent the RCD's catastrophic failures during the job. Additionally, the data is recorded to allow further processing and analysis using ML and AI techniques.

Keywords: Managed Pressure Drilling, condition monitoring, Rotating Control Device, MPD, RCD

1. Managed pressure drilling background

The primary role of the drilling mud in traditional oil and gas well drilling operations is to lubricate the bit, clean the well from the cuttings, and provide hydrostatic pressure. Traditionally, the mudflow system is open to atmospheric pressure, and drilling mud is typically the first line of the well control practice and a pressure overbalance is established with a specially selected drilling mud density to allow for safe drilling operations. However, it is estimated that around 70% of the hydrocarbon resources available offshore cannot be drilled economically using conventional drilling techniques [1].

An alternative method to control bottom hole pressure can be achieved with the Managed Pressure Drilling (MPD) technique. MPD is currently more and more widely utilized to address pressure profile uncertainty, wellbore ballooning, and loss circulation problems within the industry. The MPD equipment package includes a Rotating Control Device (RCD) and a choke manifold to establish a closed-loop system and regulate the pressure from the surface. The goals for successful MPD operations are to detect the downhole pressure environment's limitations and alter the annular hydraulic pressure profile accordingly [2]. By eliminating well control concerns and immediately altering bottom hole pressure when necessary, MPD increases safety and decreases Non-Productive Time (NPT).

The RCD is one of the most important components because it maintains a closed system by providing a pressure seal on the hydrostatic column while permitting pipe movement. The typical RCD comprises two components, as shown in Figure 1: a stationary housing called the RCD bowl that sits on top of the BOP stack and rotating seal elements with a bearing mechanism inserted inside the RCD bowl collectively known as the bearing assembly. A hydraulically actuated clamp and a safety bolt are frequently used to lock the bearing assembly in the RCD bowl. This bearing assembly provides the pressure seal and rotation, making it a closed-loop system.

The MPD significantly reduces this risk by containing the returns and diverting them away from the drilling floor, where a potential hazard of gas at the surface is continuously present during conventional drilling operations, putting the safety of the rig crew and all personnel around the rig at risk.

Additionally, the MPD systems can quickly detect the hydrocarbon influxes, giving sufficient time for the drilling crew to regain control over the well in a very short period.

Figure 2 shows the flow path through the closed RCD system, which enables drilling in a closed seal environment while rotating. The RCDs are currently manufactured and tested to the API 16 RCD, where various pressure cycling and pipe manipulation tests are required to qualify the new equipment [3]. However, during the typical MPD job, the environment and forces acting on the RCDs can differ from the environment where the RCDs were tested. As a result, there are occasions where premature RCD failures can occur. Catastrophic failures of the RCDs usually can occur without a significant warning to the operator. They can result in risky drilling scenarios such as well control issues, well stability issues, and stuck pipes.

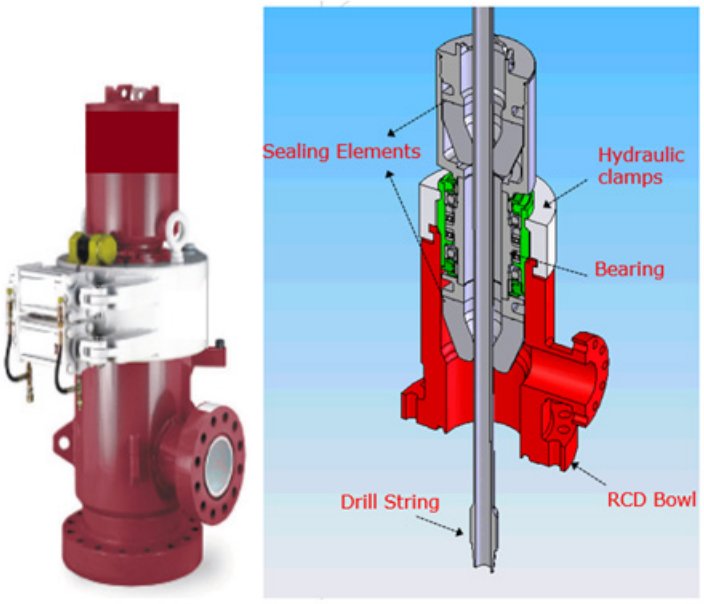

Fig. 1. Rotating Control Device assembly

Source: Weatherford

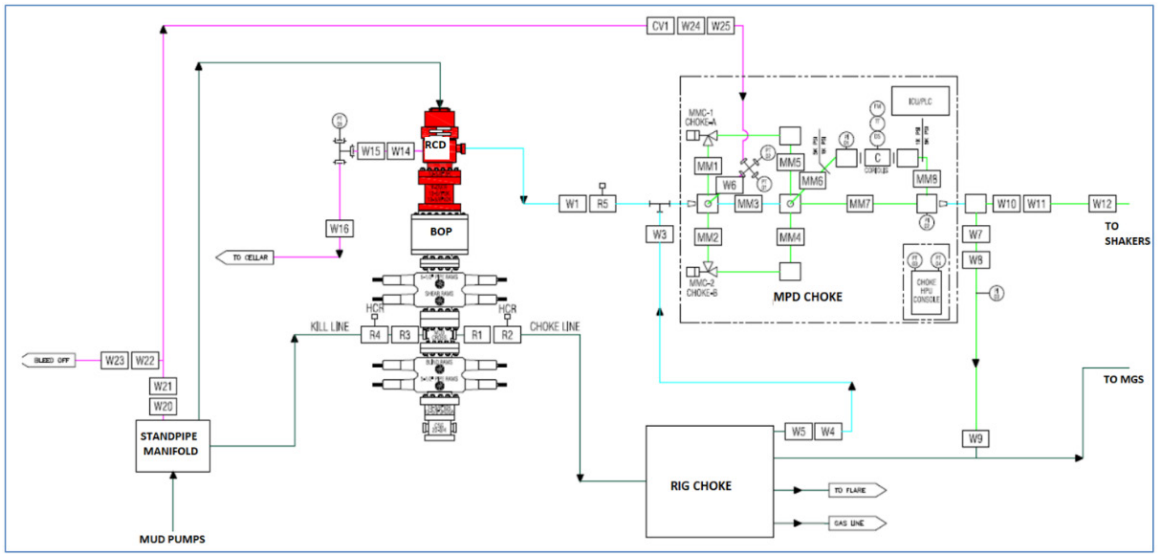

Fig. 2. RCD and MPD flow-path

Source: Weatherford

2. Common failures with RCDs

The RCD is critical equipment that enables the entire MPD technique. Even though the current operators implement strict maintenance procedures tied to the recommended hours of rotation and footage stripped threshold to avoid premature failures, there are still occasions of seal leakages and catastrophic equipment failures. The following are the most common failures:

1. RCD sealing elements leak as a result of defective seals.
2. Seizures in RCD bearings, leading to seal deterioration and leakage.

Capturing and understanding the causes that cause RCD failures is essential to increase the reliability and improve the safety of the MPD operations. Furthermore, understanding and eliminating the causes of the RCD failures can extend the RCD life and provide more conclusive recommendations for early bearing assembly replacement.

3. RCD monitoring system requirement

The continuously changing environment from one job to another for the RCDs and random failures of this equipment has encouraged developing a condition monitoring system to understand better the factors leading to premature RCD failures.

The operational requirements for such a condition monitoring system covered the necessity to operate during drilling activities covering Zone 0, Zone 1, Safe Zones, high ambient temperature, and dust particles usually preset while drilling in the desert. The new system was required to be non-intrusive to avoid any modifications to the existing MPD system and operational procedures. The newly developed system consists of a portable, add-on jacket with various sensors mounted on the RCD. This system was designed to operate in a Passive Mode, collecting data and plotting the results in real-time to the operator in the field on an integrated Human Machine Interface. At the early stage of the development, this system wasn't intended to give any suggestions to the operator to avoid potential false alarms before a sufficient data analysis was performed first.

4. Sensors and measurements

Various non-intrusive sensors are installed directly on the RCD and related MPD drilling machinery.

Figure 3 shows the position of the sensors as well as the overall clamp-on system. The sensors listed below were selected and positioned to allow for the measurement of the following:

Rotational Speed Sensor – monitoring the relative speed of rotation of the Top Drive, the drill pipe, and the RCD bearing assembly. The primary function of this sensor is to monitor for any rotational slip between these components. For example, a difference in rotational speed could suggest a problem with bearings or seals.

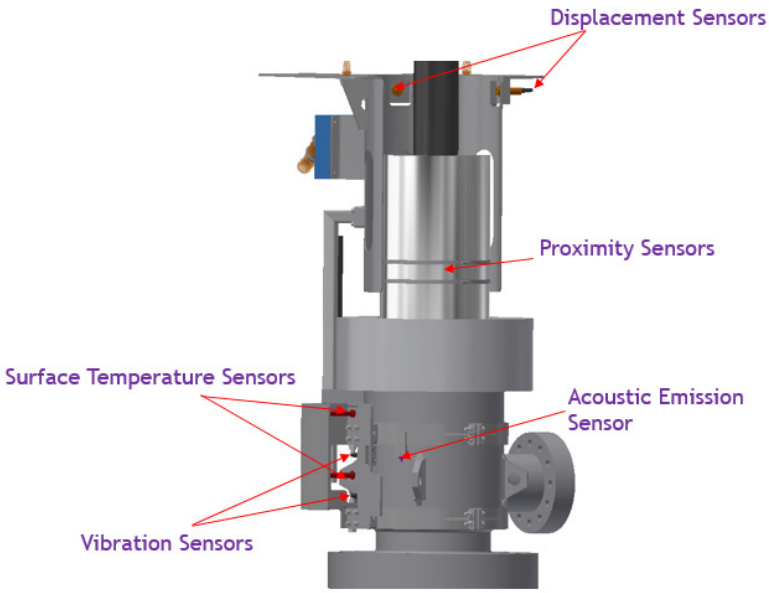

Fig. 3. 3D model of a RCD condition monitoring system mounted on a dedicated RCD

Source: Aramco Overseas Company

Displacement Sensors – monitoring the position of the drill pipe relative to a stationary datum. This is determined using an array of proximity sensors, as is the drift of drill pipes relative to the Top Drive and the RCD. Two displacement sensors are used to check for any potential misalignment between the Top Drive and the RCD. The displacement sensors also track the movement of drill pipes into and out of the well.

Vibration Sensors – the RCD's vibration sensors monitor the vibrational signature from the interactions between the seal and the drill pipes and the integrity of the RCD's bearings. Vibration data also offers information on the system's response to the ongoing drilling operations.

Temperature Sensors – measuring the RCD housing temperatures to determine any change of the conditions that can cause temperature change inside the housing, which are not dependent on the environmental temperature changes. It is expected that some temperature changes might come from the change of the friction factor in the bearings and the seals or temperature changes of the drilling fluids.

Acoustic Emissions Sensor – mounted on the housing, attempts to detect acoustic-related events related to the RCD responses due to drilling events and the seal and bearing element condition.

Each sensor is connected to Data Acquisition System. The system design allows storing raw data from the sensing equipment with a corresponding time and date stamp. The data is saved on various mediums, including integrated local storage, removable SD as a backup, and removable USB for further data analysis. Simplified data processing was applied at this early phase. Data from the sensors is processed locally within the central unit. Results are displayed to the operator in real-time in two primary forms: pre-set level alarms and visual graphs that monitor trend deviations. Collected data is displayed on an integrated display on the central unit Human Machine Interface (HMI), allowing the operator to interact with the system, read and adjust the alarm levels, modify graphs for more precise analysis, set some basic parameters, download data to USB.

The processed data is used to trigger simple alarms and to provide feedback to the operator. These alarms are communicated to the operator in the form of visual and sound events. At the early stage, they help with self-troubleshooting the system by detecting any readings significantly off the scale to check the system and sensors if they are functioning correctly. All the collected RAW data can be transferred directly from the central unit to a dedicated device for more sophisticated analysis.

5. On-field installation and operation

The condition monitoring system was created with the user in mind, making it simple to set up and appropriate for usage in a Zone 1 hazardous area during drilling activities. All the sensors were pre-attached to an add-on jacket to allow easy installation to the RCD bowl, along with a certified junction box for hazardous conditions to gath-

er signals from each of the sensors. The junction box was connected to the HMI and powered with the aid of a multicore cable. The HMI was placed inside the MPD container providing shelter against the high temperatures and significant dust usually present in desert environments.

This new equipment was complemented with monthly tests checks and the maintenance schedule, ensuring the equipment's durability even in the most extreme conditions.

6. Data from first jobs and results

The RCD condition monitoring system has been successfully deployed and tested during the MPD job in the field. The initial field testing was mainly focused on assessing the successful development of the entire system and confirming the whole package is functioning correctly. All the sensors have successfully communicated with the data gathering unit. As a result, the main measurements were in the expected ranges, and graphical charts with data were obtained on the HMI display on the data acquisition system available to the MPD operator during the job.

Essential sensor readings were acquired, downloaded, and shared to seek potential system upgrades, apparent trend deviations, and plan for more sophisticated data analysis. Figure 4 shows a visual representation of the gathered data gathered from the system during an MPD job.

During the first field deployments, various drilling events were observed, recorded, and displayed to the operator in real-time. During the specific drilling activities, specific trends were starting to form.

The system has recorded unique signatures related to running pipes in the hole, drilling, and pulling pipes out of the hole. The proximity sensors detected the tool joints passing through the RCDs, allowing calculating the tripping pipe speeds. Corresponding vibration signatures were also recorded with changes related to the different drilling activities. These readings were successfully displayed to the operator in real-time during the job.

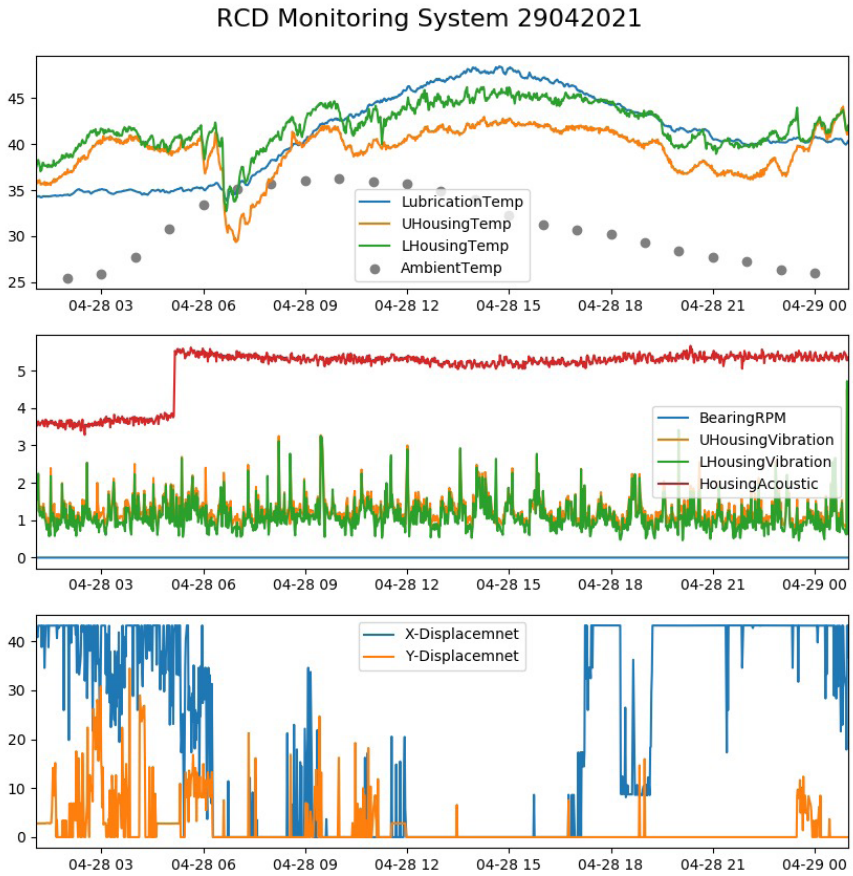

Fig. 4. Collected data displayed on a three charts

Source: Aramco Overseas Company

7. Summary and conclusions

The RCD monitoring system is an add-on jacket designed to be installed on the RCDs, in the field, during the MPD jobs to monitor their health. All sensors included within this system are non-intrusive sensors. They allow monitoring temperatures, vibration, acoustic emissions, pipe-RCD misalignment, and RCD-pipe relative rotations. The readings are presented to the operator in an easy-to-understand format to alert the operator about any substantial trend deviations and prevent catastrophic failure. The data acquired will be used in later stages to predict the time-to-failure of the RCD in bearing and seal elements, allowing for safe corrective steps. Currently, the system is operating in a passive mode, collecting data. More data is being collected in additional field jobs to improve data analysis, identify applicable trend deviation limits, and predict a safe operating window for critical MPD operations. In addition, more data is expected to aid in quantifying the health of the RCD sealing and bearing components.

References

[3] Coker I.C.: *Managed Pressure Drilling Applications Index.* OTC-16621-MS Presented at Offshore Technology Conference, Houston, Texas, May 2004.

[4] Al Marhoon Z.: *The Effect of Pipe Rotation on Dynamic Well Control Casing Pressure within MPD Applications*. Louisiana State University 2018.

[5] American Petroleum Institute: *API Specification 16 RCD. Specification for Rotating Control Devices*. 2nd Edition, September 2015.